EFDA–JET–PR(12)62

T. Craciunescu, A. Murari, I. Tiseanu, J. Vega
and JET EFDA contributors

Phase Congruency Image Classification for MARFE Detection at JET

Phase Congruency Image Classification for MARFE Detection at JET

T. Craciunescu[1], A. Murari[2], I. Tiseanu[1], J. Vega[3]
and JET EFDA contributors*

JET-EFDA, Culham Science Centre, OX14 3DB, Abingdon, UK

[1]EURATOM-MEdC Association, NILPRP, Bucharest, Romania
[2]Consorzio RFX, Associazione EURATOM-ENEA per la Fusione, Padova, Italy
[3]Asociación EURATOM/CIEMAT para Fusión, Madrid, Spain
** See annex of F. Romanelli et al, "Overview of JET Results",*
(23rd IAEA Fusion Energy Conference, Daejon, Republic of Korea (2010)).

Preprint of Paper to be submitted for publication in Proceedings of the
11th Kudowa Summer School, "Towards Fusion Energy"
Kudowa Zdrój, Poland June 11th June - 15th June 2012

ABSTRACT

MARFE instabilities may reduce confinement leading to harmful disruptions. They cause a significant increase in impurity radiation and therefore they leave a clear signature in the video data. This information can be exploited for automatic identification and tracking. A MARFE classifier, based on the phase congruency (PhC) theory, has been developed and adjusted to extract the structural information in the images of JET cameras. This approach has the advantage to use a dimensionless quantity and to provide information that is invariant to image illumination, contrast and magnification. The method is tested on JET experimental data and has proved to provide a good prediction rate.

1. INTRODUCTION

Video cameras have recently become diagnostic tools widely used on Joint European Torus (JET) for fusion plasma diagnostic and control. Camera based instruments provide essential information for both the control of the experiments and the physical interpretation of the results. These cameras can produce up to hundreds of kframes per second and their information content can be very different, depending on the experimental conditions. However, the relevant information about the underlying processes is generally of much reduced dimensionality compared to the recorded data. The extraction of the relevant information, which allows the full exploitation of these diagnostics, is a challenging task.

Recently, several methods were developed for the automatic identification and tracking of objects in videos. A complete MARFE identifier, based on morphological operators and Hu moments [1], and a MARFE tracking method, based on the motion estimation within the MPEG video compressed domain [2], were reported. These methods can be applied to explore JET database for retrieving specific events needed for physical studies.

The real-time detection is extremely important as these instabilities may trigger harmful disruptions. Currently, at JET, the fast imaging systems are not yet used for their real time control. Two main aspects will have to be solved to use fast cameras for protection and control: the streaming of the data in real time and the developments of image processing algorithms fast and accurate enough to extract the relevant information. This paper deals only with the second class of issues.

Several approaches, which aim to use the video data for the real time identification of MARFE have been reported in the literature. A hardware solution is based on the real-time image processing capability of cellular nonlinear/neural network-based chips [3]. A highly parallelized software implementation of the method introduced in Ref. 1 was recently reported [4].Although a good rate of correct classifications and high speed implementations were achieved by the above mentioned methods, the problem remains open for approaches based on different paradigms which may lead to further improvements. In this paper we report first results obtained by using the phase congruency (PhC) theory.

PhC theory is based on physiological and psychophysical evidences which show that visually discernable feature coincides with those points where the Fourier waves, at different frequencies,

have congruent phases. PhC was introduced by Morrone et al. [5] and it provides a simple but biologically plausible model of how mammalian visual systems detect and identify features in an image. The extraction of features at points of high PhC is sustained by some recent studies in neurobiology using functional magnetic resonance imaging [6]. PhC has the advantage to be a dimensionless quantity and to provide information that is invariant to image illumination, contrast and magnification.

PhC was used in the past as a tool for several image features significance estimation [7-10]. Recently, it was brought back into attention together with the development of Image Quality Assessment (IQA) methods. IQA methods attempt to quantify the differences between a distorted image and a reference image using a variety of known properties of the human visual system. The interest for accurate and easy to use IQA methods increased dramatically in a wide range of application like image acquisition, transmission, compression, restoration and display. Several IQA methods make use of the assumption that the human visual system is adapted to the structural information in images. The visual information in an image is often very redundant, but the human visual system understands the image mainly based on its low-level features, such as edges and zero-crossing. A measurement of structural similarity should provide a good approximation of perceived image quality. PhC, as a dimensionless measure of the significance of a local structure was used as a component in defining the FSIM (Feature Similarity Index) index [11]. A similarity score was developed based on the cross correlation between partitioned PhC maps [12]. PhC was extended to phase coherence in order to characterize the image blur [13] and sharpness [14].

The ability of PhC to extract highly informative features is used in our approach for MARFE automatic identification by full reference similarity. Reference 'pristine' MARFE frames are used in order to identify distorted or displaced similar patterns in input video data. The PhC concept and its implementation for MARFE automatic identification is presented in Section 2. Experimental results and the method assessment are presented in section 3.

2. METHODS

2.1 PHASE CONGRUENCY

Morrone and Owens [15] define the PhC function in terms of the Fourier series expansion of a signal at some location x as:

$$PC\,(x) = max_{\bar{\phi}(x)\,\in\,[0.2\pi]} \frac{\Sigma_n A_n cos\,(\phi_n(x) - \bar{\phi}_n(x))}{\Sigma_n A_n} \tag{1}$$

where: A_n represents the amplitude of the n-th Fourier component, $\phi_n(x)$ represents the local phase of the Fourier component at position x and $\bar{\phi}_n(x)$ is the mean local phase angle of all the Fourier terms at the position x. The construction of PhC from the Fourier components is illustrated in Fig.1.

An alternative approach is to calculate points of maximum PhC by searching for peaks in the local energy function, which is defined by the following relation:

$$E(x) = \sqrt{F(x)^2 + H(x)^2} \tag{2}$$

where $F(x)$ is the signal with its DC component removed, and $H(x)$ is the 90 deg. phase shift of $F(x)$ (the Hilbert transform). The energy is equal to phase congruency scaled by the sum of the Fourier amplitudes [16]:

$$PhC(x) = \frac{E(x)}{\Sigma_n A_n} \tag{3}$$

Approximations of $F(x)$ and $H(x)$ can be obtained by convolving the signal with a quadrature pair of filters. Linear-phase filters must be used in order to preserve phase information. A widely used approach is represented by nonorthogonal wavelets that are in symmetric/antisymmetric quadrature pairs [17]. Let Q^n_{even} and Q^n_{odd} be the the even-symmetric and odd-symmetric filters on scale n and let be $[e_n(x), o_n(x)]$ the responses of the quadrature pairs to a 1-D signal Ix. The local amplitude on scale n is given by the relation:

$$A_n = \sqrt{e_n(x)^2 + o_n(x)^2} \tag{4}$$

and the energy components are:

$$F(x) = \Sigma_n e_n(x), \qquad H(x) = \Sigma_n o_n(x) \tag{5}$$

Therefore the 1-D PhC can be calculated as:

$$\mathrm{PhC}(x) = \frac{E(x) - T}{\Sigma_n A_n(x) + \varepsilon} \tag{6}$$

where:

- ε is a small positive constant introduced in order to address the case when all the Fourier amplitudes are very small, and therefore the PhC calculation become ill conditioned.
- T is a multiple of the mean noise response; T is introduced in order to eliminate spurious responses to noise. It ensures that PhC of a legitimate feature is significant relative to the level of noise.

PhC is significant only if it occurs over a wide range of frequencies, for a specific location. Therefore a multiplicative weighting factor w (x) must be introduced in (6), in order to penalize PhC at locations where the spread s (x) of the filter responses is narrow. Kovesi [18] suggested that a measure of filter response spread can be achieved by the following relation:

$$s(x) = \frac{1}{N} \frac{\Sigma_n A_n(x)}{A_{max}(x)(x)} \tag{7}$$

where N is the total number of scales being considered and Amax(x) is highest individual response at x. The weighting function is constructed by applying a sigmoid function to the filter response spread value:

$$w(x) = \frac{1}{1 + e^{\gamma(c - s(x))}} \tag{8}$$

where *c* is the cut-off value of the filter response spread below which phase congruency values become penalized, and γ is a gain factor that controls the sharpness of the cutoff.

The PhC calculation for 2-D images is obtained by applying 1-D calculation over several orientations and combining the results in some appropriate way. A lateral extension of the filters is introduced by mean of a spreading function applied across the filter, perpendicular to its orientation. An appropriate choice is the Gaussian function which may induce amplitude modulation in the image, but leaves the phase unaffected. Therefore it ensures PhC preservation any features in the image.

An adequate solution for constructing the symmetric/antisymmetric quadrature pairs of filters are the Gabor filters. These filters became popular in image vision partly because Daugman [19-20] showed that the receptive fields of most orientation receptive neurons in the (cat's) brain looked very much like Gabor functions. In the spatial domain, a 2-D Gabor filter is a Gaussian kernel function modulated by a sinusoidal plane wave. This filter will therefore respond to some frequency, but only in a localized part of the signal (see e.g. Ref. 21 for a detailed discussion). The Gabor filters are self-similar: all filters can be generated from one mother wavelet by dilation and rotation. Self-similarity leads to a straightforward implementation over several scales and orientations. The main limitation resides in the impossibility of ensuring both an arbitrarily wide bandwidth and a reasonably small DC component. The transfer function of an even-symmetric Gabor filter, in the frequency domain is the sum of two Guassians (centered at plus and minus centre frequency). The two Gaussians overlap, leading to a non-zero DC component.

An improved alternative to the Gabor function is the log-Gabor function proposed by Field [22]. Field suggests that natural images are better coded by filters that have Gaussian transfer functions when viewed on the logarithmic frequency scale. Log-Gabor filters can be constructed with arbitrary bandwidth which can be optimized to produce a filter with minimal spatial extent. On the linear frequency scale, the log-Gabor function has a transfer function of the form:

$$G(\omega) = e^{-\frac{\left(\log \frac{\omega}{\omega_0}\right)^2}{2\left(\log \frac{k}{\omega_0}\right)^2}} \tag{9}$$

where ω_0 is the filter's centre frequency. To obtain constant shape ratio filters the term k/ω_0 must also be held constant for varying ω_0. By definition, the log-Gabor function has no DC component. The transfe function has an extended tail at the high frequency end, preventing the under-representation of high frequency components.

By using Gaussians as spreading functions, the 2D log-Gabor function is defined by the following relation:

$$G_{2D} = e^{-\frac{\left(\log \frac{\omega}{\omega_0}\right)^2}{2\sigma_\Gamma^2}} \times e^{-\frac{(\theta-\theta_j)^2}{2\sigma_\Gamma^2}} \tag{10}$$

Where $\sigma_R = \log {}^{k}/_{\omega_0}$, θ_j is the j-orientation angle of the filter and θ_σ determines the filter's angular bandwidth.

The PhC values obtained for different orientations have to be combined ensuring that features or conjunction of features, at all orientations, are treated equally. This can be achieved by summing and normalization over all orientations and scales:

$$PhC\ (x) = \frac{\Sigma_o \Sigma_n\ w_{no}\ (x)\ E_{no}\ (x) - T}{\Sigma_o \Sigma_n\ A_{no}\ (x) + \varepsilon} \tag{11}$$

PhC can be used to identify significant features in the image as it values varies between 0 (a feature with no significance) and 1 (a very significant feature).

2.2 MARFE AUTOMATIC IDENTIFICATION

The MARFE instability is a tokamak edge phenomenon characterized by greatly increased radiation, density and density fluctuations, and decreased temperature in a relatively small volume. MARFE usually occur on the high field side of the torus [23] and are the manifestation of a thermal instability, with impurity radiation being the main energy loss mechanism from its volume. MARFEs can reduce confinement and, more importantly, they can cause disruptions which lead to the sudden losses of plasma confinement which determine the abrupt end of the discharge. They may represent a risk for the integrity of the devices. As MARFEs cause a significant increase in impurity radiation, they leave a clear signature in the videos recorded by visible cameras: they appear as ribbons of radiations moving up and down the vacuum vessel on the high field side. A typical MARFE sequence of images recorded at JET is presented in Fig.2. For the JET database, the video signature is visible for a number of frames between 3 and 65 [10].

Some specific MARFEs characteristics can be exploited for automatic identification. MARFEs are characterized by their top-to-bottom movement, and they have a clearly defined ribbon-like shape, at least for the first part of the movement (Fig.2). However, the identification method must be able to avoid the confusion with other video objects, like e.g. flashes, probably caused by ELMs (Edge Localized Modes) or high radiation from the poloidal limiters.

A region of interest can be defined to encompass the area corresponding to the first part of the evolution of a MARFE (Fig.4). PhC is calculated over several orientations θ_k (Fig.4). PhC is evaluated for the current frame in the input video data and also for one or more reference frames, over several orientations θ_k, determined by the MARFE ribbon-like shapes (Fig.4).

A similarity map between these frames can be constructed using the following relation [24]:

$$\mathrm{SIM}\,(x) = \frac{2 \cdot \mathrm{PhC}_i^{cur} \cdot \mathrm{PhC}_i^{ref} + T'}{(\mathrm{PhC}_i^{cur}) + (\mathrm{PhC}_i^{ref})^2 + T'} \tag{12}$$

where Im_{cur} is the current image, Im_{ref} is the reference image and T′ is a positive constant introduced in order to ensure the stability of the calculation of SIM. The *SIM* map contains similarity values for each location x, ranging within (0, 1]. For multiple reference images PC^{ref_j} (j = 1,..,N) the corresponding similarity indexes SIM_j are multiplied in order to obtain a global structural similarity map:

$$SIM\,(x) = \prod_j^N SIM_j\,(x) \tag{13}$$

where is the total number of reference images.

The *SIM* map, which contains similarity values calculated at each location x can be pooled into a single similarity score using the relation:

$$SIM_{score} = \frac{1}{D} \int_{x \in \Omega} SIM\,(x)\,dx \tag{14}$$

where Ω is the map domain and D is its area.

3. RESULTS

The PhC image classification method has been implemented following the steps described previously.

For each analyzed image, the PhC evaluation implies the calculation of its Fourier transform, and the convolution with the pre-calculated odd and even filter components, at each scale. The amplitudes of odd and even responses are used for the calculation of energy (Eq.2) and PhC (Eq.6) values. We used a total number of 4 wavelet scales and a scaling factor of 2 between successive filters. The ratio of the standard deviation of the Gaussian describing the log Gabor filter's transfer function in the frequency domain to the filter center frequency is $k/\omega_0 = 0.5$ (Eq.9). The standard deviation for the angular filter component is $\sigma_\theta = 1.3$.

The noise affecting the signal may have a significant influence on the PhC behavior due to the normalization used in Eq.6. Therefore a careful evaluation of the factor T (Eq.6), introduced in order to ensure that PhC is significant in respect to the noise level, must be ensured. A detailed procedure is described in Ref. 18. It assumes that the noise is Gaussian with random phase and it is based on the estimation of the influence of noise in the calculation of the energy E (x) (Eq. 2). The influence of the image noise is estimated from the response of the smallest scale filter pair, which has the largest bandwith, and therefore, it gives the strongest noise response. The response across the whole image will be primarily determined by the noise distribution. The response will differ only at feature points in the image. However features occur at isolated locations in the image and the wavelet have a small extent at this scale. Therefore the influence on the noise induced by the

filters response to feature in the image may be judged as a limited contamination. This procedure has proved to be very efficient. However, as it must be applied for each analyzed image it leads to supplementary computing time. A systematic analysis of the results provided by this procedure has been performed in order to determine an empirical constant value $T = 0.85$, able to efficiently eliminate spurious responses to noise, applicable for all the videos containing MARFE events.

The parameters of the frequency spread weighting function (8) have been set to $c = 0.5$ and $\gamma = 10$. The value of the constant introduced in order to address the case when the all the Fourier amplitudes are very small (Eq. 6), has been set to $\varepsilon = 0.001$.

The method has been tested on videos extracted from the JET database. All the videos were recorded using the wide angle view fast visible camera (Photron APX) installed in the Joint European Torus JET [25]. The camera is installed on the arm of the IR endoscope and it is viewing the full poloidal crosssection of the vacuum vessel and is covering a toroidal extent of ~90^{o}. The wide angle view is appropriate for the study of pellet ablation, large scale instabilities and plasma wall interactions. The experimental data used in this paper contains a total number of 11500 frames, ~14.1% represent MARFE events and ~2.8% displays non-MARFE events (ELMs, UFOs etc).

For all these video frames the PhC analysis was performed for a maximum number of four orientations. This number of orientations proved to be sufficient to provide enough detailed information for natural image quality assessment of images [17]. However, as the computation time depends strongly on the number of orientations, a detailed analysis of the performances of the method in respect with this parameter has been performed. This analysis has proved that good results can be obtained using only two orientations.

A representative result is illustrated in Fig. 5 for JET pulse #50053. The evolution of the similarity score SIM_{score} is characterized by clearly revealed peaks corresponding to MARFE events (peaks M1÷M7). A threshold level, can be introduced to separate peaks corresponding to MARFE events from non-MARFE ones (peak E). Taking into account all the videos analyzed, it results that the threshold value can be set anywhere in the range $SIM_{score} \in 0.900 \div 0.904$. If the severe degradation of the image quality of several frames (like e.g. M_1 and M_6), due to camera artifacts, can be avoided, the range can be significantly increased $SIM_{score} \in 0.900 \div 0.965$. This will allow a more reliable discrimination of MARFE events.

The developed classifier, adapted to the structural information in images, ensures a good prediction rate. For the videos used in the experiments reported here, 96.2% are correctly interpreted. From the misclassified events 0.03% are false positives and 3.5% false negatives.

CONCLUSION

A method based on PhC principle has been developed for MARFE automatic identification. The method combines PhC information over multiple orientations creating a highly localized operator, with increased values at locations with increased structural significance. PhC has the advantage to be invariant to contrast and luminosity and therefore can work well with JET videos, which can

be affected by a variable background. PhC proved to be robust with respect to the distortion and magnification of MARFE's shapes. A good prediction rate is achieved.

The method depends on several adjustable parameters. However, once tuned, they remain valid for all JET videos. An effort has been devoted to the optimization of the computation complexity. Further work will be dedicated to investigating the possibility of an implementation compatible with online MARFE identification. As mentioned also in the introduction, this will require also an upgrade of the hardware of the cameras since the one presently used and with the right time resolution to identify MARFEs cannot perform real time streaming of the videos.

ACKNOWLEDGMENT

This work was supported by the European Communities under the contract of Association between EURATOM and MEdC, ENEA and CIEMAT and was carried out within the framework of the European Fusion Development Agreement. The views and opinions expressed herein do not necessarily reflect those of the European Commission.

REFERENCES

[1]. A. Murari, M. Camplani, B. Cannas, D. Mazon, F. Delaunay, P. Usai, and J. Delmond, "Algorithms for the automatic identification of MARFEs and UFOs in JET database of visible camera videos," IEEE Trans. On Plasma Science, vol. **38**, no. 12, pp. 3409–3418, 2010.

[2]. T. Craciunescu, A. Murari, I. Tiseanu, P. Lang, Motion estimation within the MPEG video compressed domain for JET plasma diagnostics, Nuclear Instruments and Methods in Physics Research A, Volume **659**, Issue 1, p. 467-476.

[3]. G. Vagliasindi, A. Murari, P. Arena, L. Fortuna, G. Mazzitelli, Cellular Neural Network Algorithms for Real-Time Image Analysis in Plasma Fusion, Instrumentation and Measurement, IEEE Transactions on Volume: **58**-8(2009)2417 – 2425.

[4]. M. Portes de Albuquerque, A. Murari, M. Giovani, N. Alves Jr., Marcelo P. de Albuquerque, A 10,000 images per second parallel algorithm for real time detection of MARFEs on JET, submitted to IEEE Transactions on Plasma Science.

[5]. M.C. Morrone, A. Navangione, and D. Burr. An adaptive approach to scale selection for line and edge detection. Pattern Recognition Letters, **16**:667–677, 1995.

[6]. R.A. Owens, S. Venkatesh, and J. Ross. Edge detection is a projection. Pattern Recognition Letters, **9**:223–244, 1989.

[7]. S. Venkatesh and R. Owens. On the classification of image features. Pattern Recognition Letters, **11**:339–349, 1990.

[8]. B. Robbins and R. Owens. 2-D feature detection via local energy, Image and Vision Computing, **15**(5):353–368, May 1997.

[9]. Peter Kovesi, Proc. VIIth Digital Image Computing: Techniques and Applications, Sun C., Talbot H., Ourselin S. and Adriaansen T. (Eds.), 10-12 Dec. 2003, Sydney, pp 309-318.

[10]. M.C. Morrone and D.C. Burr, Feature detection in human vision: a phase-dependent energy model, Proc. R. Soc. Lond. B, 235-1280(1988) 221-245.

[11]. L. Zhang, L. Zhang, X. Mou, D. Zhang, FSIM: A Feature Similarity Index for Image Quality Assessment , IEEE Transactions on Image Processing, 20-8(2011)2378-2386.

[12]. Z. Liu and R. Laganière, "Phase congruence measurement for image similarity assessment", Pattern Recognit. Letters, **28**-1(2007)166-172.

[13]. Z. Wang and E.P. Simoncelli, Local phase coherence and the perception of blur, in Adv. Neural Information Processing Systems., 2004, pp. 786-792.

[14]. R. Hassen, Z. Wang, and M. Salama, No-reference image sharpness assessment based on local phase coherence measurement, in Proc. IEEE Int. Conf. Acoust., Speech, and Signal Processing, 2010, pp. 2434-2437.

[15]. M.C. Morrone and R.A. Owens, Feature detection from local energy, Pattern Recognit. Letters, vol. **6**, no. 5, pp. 303-313, Dec. 1987

[16]. S. Venkatesh and R. A. Owens. An energy feature detection scheme.In The International Conference on Image Processing, pages 553–557, Singapore, 1989.

[17]. J. Morlet, G. Arens, E. Fourgeau, and D. Giard. Wave propagation and sampling theory - Part II: Sampling theory and complex waves. Geophysics, **47**(2):222–236, February 1982.

[18]. P. Kovesi, Image features from phase congruency, Videre: International Journal of Computer Vision, vol. **1**, no. 3, pp. 1-26, 1999.

[19]. J.G. Daugman, Two dimensional spectral analysis of cortical receptive field profiles, Vision Res., 20(1980)847- 856.

[20]. J.G. Daugman, An information–theoretic view of analogue representation in striate cortex, Computational Neuroscience, Ed. Schwartz, E. L., Cambridge, MA: MIT Press, 403–424, 1990.

[21]. A. Lagae, S. Lefebvre, G. Drettakis, P. Dutre, Procedural Noise using Sparse Gabor Convolution, ACM Transactions on Graphics **28**, 3 (2009) 54-64.

[22]. D. Field. Relations between the statistics of natural images and the response profiles of cortical cells. Journal of the Optical Society of America A (**4**):2379 – 2394, 1987.

[23]. H.B. Lipschultz, B. LaBombard, E.S. Marmar et al., "MARFE: An Edge Plasma Phenomenon", Nuclear Fusion, vol. **24**-8(1984) 977-988.

[24]. Z. Wang, A.C. Bovik, H.R. Sheikh, and E.P. Simoncelli, "Image quality assessment: From error visibility to structural similarity," EEE Transactions on Image Processing., vol. **13**, no. 4, pp. 600–612, Apr. 2004.

[25]. J.A. Alonso, P. Andrew, A. Neto, J.L. de Pablos, E. de la Cal, H. Fernandes, J. Gafert, P. Heesterman, C. Hidalgo, G. Kocsis, A. Manzanares, A. Murari, G. Petravich, L. Rios, C. Silva, P.D. Thomas, Fast visible camera installation and operation in JET, International Conference on Burning Plasma Diagnostics, Varenna, Italy, 24–28 Sept. 2007, AIP Conf. Proc. 988, pp. 185-188.

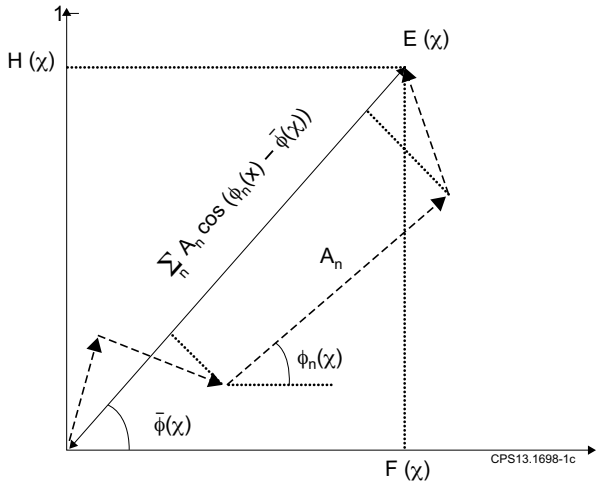

Figure 1: Illustration of the construction of PhC. The local Fourier components, at a specific location x, are plotted as complex vectors adding head to tail. The energy of the signal E (x) and its components F (x) - the signal with its DC component removed and H (x) - the Hilbert transform of F (x) are shown.

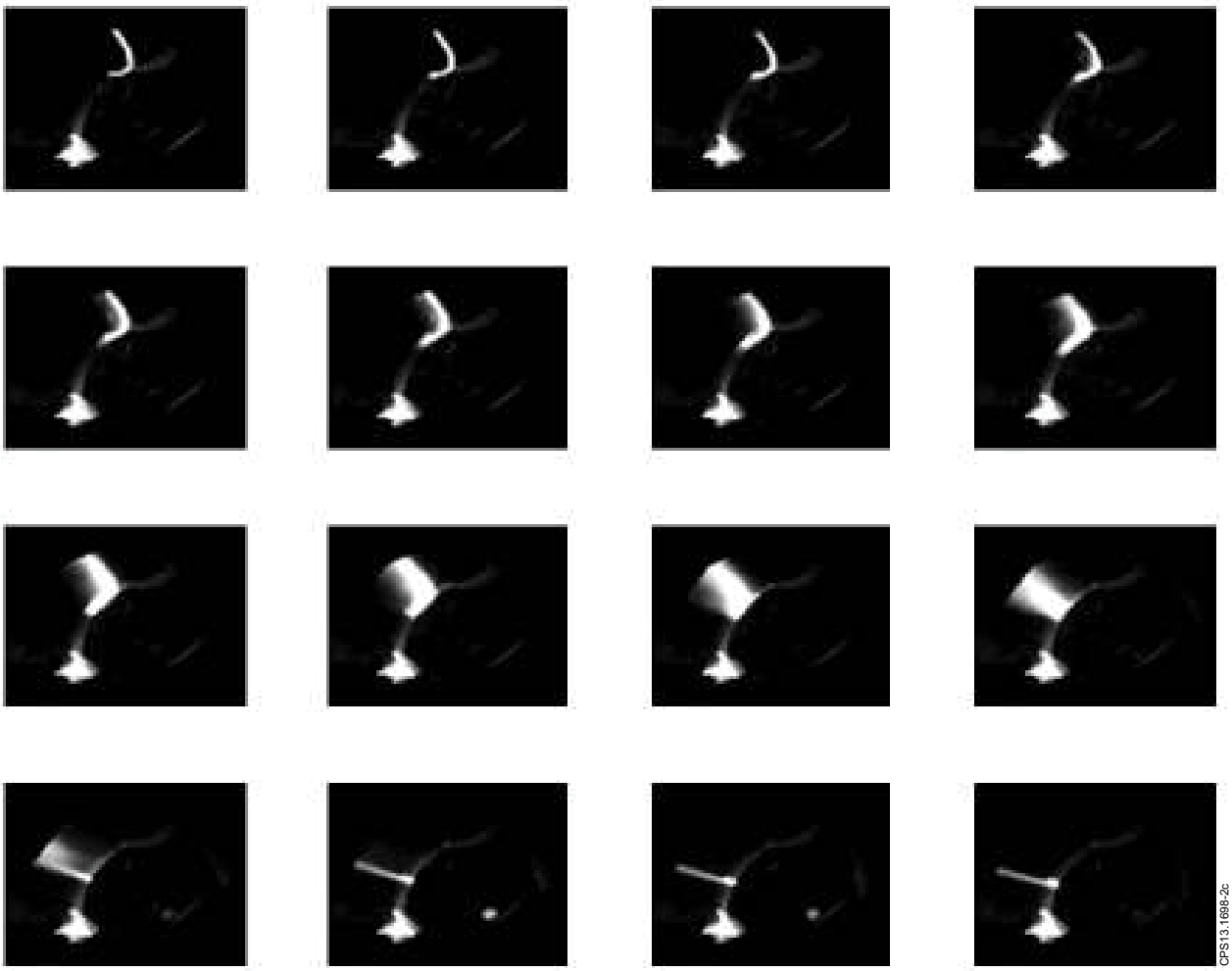

Figure 2: MARFE image sequence recorded during JET Pulse No: 70050 during the time interval 13.869477-13.869953s (frames 1621-1636).

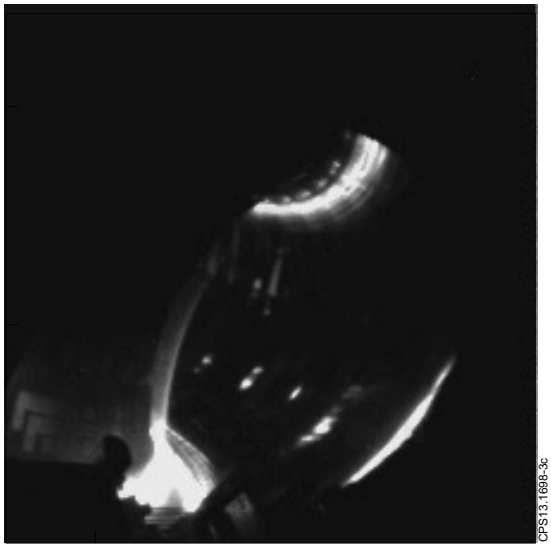

Figure 3: Video frame showing a video shape similar to a MARFE one.

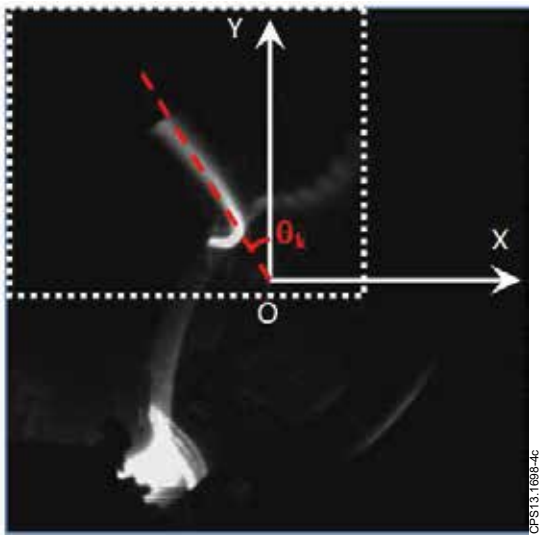

Figure 4: A region of interest (dotted square) and a particular orientations kl used for the calculation of PhC.

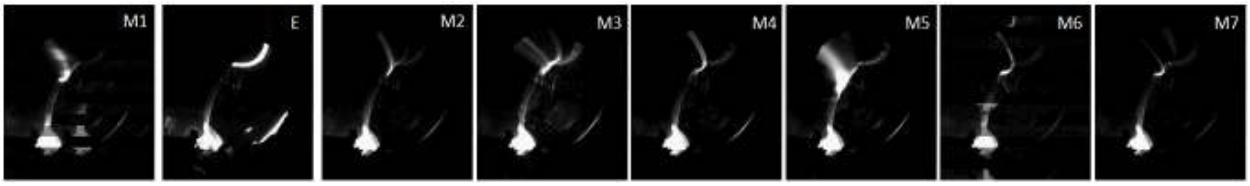

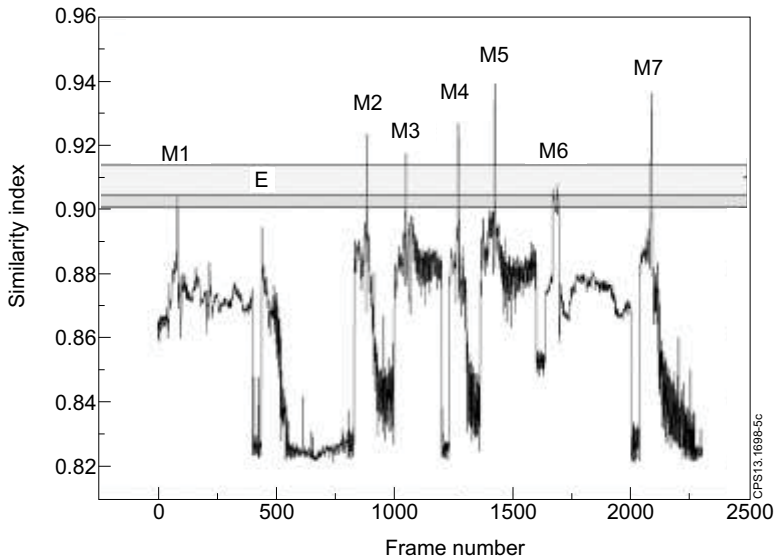

Figure 5: The evolution of the similarity score SIM_{score} for JET Pulse No: 50053. The range in the SIM_{score} where a threshold level can be introduced to separate peaks corresponding to MARFE events (peaks M1,…M7) from non-MARFE ones (peak E) is represented: i) dark gray band for the all videos, no matter of the image quality and ii) light gray band for the case when frames affected by camera artifacts are removed.